Journal of Power Sources 254 (2014) 277–286

Contents lists available at ScienceDirect

Journal of Power Sources

journal homepage: www.elsevier.com/locate/jpowsour

Experimental testing procedures and dynamic model validation for vanadium redox flow battery storage system

Francesco Baccino [a], Mattia Marinelli [b], Per Nørgård [b], Federico Silvestro [a,*]

[a] DITEN – Naval Architecture, Electrical, Electronics and Telecommunication Engineering Department, University of Genoa, via all'Opera Pia 11a, 16145 Genoa, Italy

[b] Department of Electrical Engineering, Technical University of Denmark (DTU) Risø Campus, Frederiksborgvej 399, Building 776, Roskilde, Denmark

HIGHLIGHTS

- Integration of renewable sources requires validated storage systems' models.
- The paper presents a characterization of a VRB storage system model.
- The dynamic model parameters are tuned according to experimental tests.
- The work has validated the model that is also suitable for other storage types.

ARTICLE INFO

Article history:
Received 6 August 2013
Received in revised form
6 December 2013
Accepted 17 December 2013
Available online 27 December 2013

Keywords:
Energy storage
Batteries
Modeling
Vanadium redox flow battery

ABSTRACT

The paper aims at characterizing the electrochemical and thermal parameters of a 15 kW/320 kWh vanadium redox flow battery (VRB) installed in the SYSLAB test facility of the DTU Risø Campus and experimentally validating the proposed dynamic model realized in Matlab-Simulink. The adopted testing procedure consists of analyzing the voltage and current values during a power reference step-response and evaluating the relevant electrochemical parameters such as the internal resistance. The results of different tests are presented and used to define the electrical characteristics and the overall efficiency of the battery system. The test procedure has general validity and could also be used for other storage technologies.

The storage model proposed and described is suitable for electrical studies and can represent a general model in terms of validity. Finally, the model simulation outputs are compared with experimental measurements during a discharge–charge sequence.

1. Introduction

Among the large variety of solutions for the integration of renewable energy systems, a crucial role is played by storage systems.

The coupling of wind and solar generation to storage systems is considered an interesting application to pursue the full exploitation of non-programmable renewable generation capabilities. Instead of curtailing the power production or shedding non-critical loads, the storage systems can deal with these issues; moreover, they can be a successful solution for large investments in grid infrastructure for reliability improvement and smart grid initiatives [1–3].

Each storage solution has some technical and economic constraints (such as size, portability, safety, efficiencies, reliability, etc.) that make it practical or feasible for only a limited range of applications [4–7].

The development of the vanadium redox flow battery (VRB) is expanding the possibilities for large-scale storage facilities, which are suitable for modern power systems. VRBs have already been used in numerous demonstration applications, and it is believed that the technology is close to being viable for a more widespread use [8–10]. It has also been reported in numerous projects that VRB technology can be successfully utilized in RES integration. In Ref. [11], a simulation model of a 10-kW VRB system was developed for wind integration. While in Ref. [12] the production of a microgrid was controlled by the proper management of the VRB output.

* Corresponding author. DITEN – via all'Opera Pia 11a, 16145 Genoa, Italy. Tel.: +39 010 3532380; fax: +39 010 3532700.
E-mail addresses: francesco.baccino@unige.it (F. Baccino), matm@elektro.dtu.dk (M. Marinelli), pern@elektro.dtu.dk (P. Nørgård), federico.silvestro@unige.it (F. Silvestro).

0378-7753/$ – see front matter © 2013 Elsevier B.V. All rights reserved.
http://dx.doi.org/10.1016/j.jpowsour.2013.12.078

The main advantages of the VRB reside in its long life and independence from energy and power ratings. Moreover, the design simplicity and ease of operation, due to the fact that the same electrolyte is used for both the positive and negative sides, make it a very promising technology.

The flow battery converts the energy stored in a liquid electrolyte into electricity. The active material for both the positive and negative electrodes of the VRB is made up of vanadium ions that are dissolved in sulfuric acid and serve as metal ions with a changing valence number. Flow batteries essentially consist of three key elements: the cell stacks, where power is converted from an electrical form to a chemical form; the tanks of electrolytes, where the energy is stored; and the circulating pumps and control systems. They differ from conventional batteries in two ways. First, the reaction occurs between two electrolytes, rather than between an electrolyte and an electrode. Second, the two electrolytes are stored externally to the cells and circulated through the cell stack as required. The great advantage that this system provides is that the electrical storage capacity is only limited by the capacity of the electrolyte storage reservoirs.

An individual cell consists of a negative electrode and a positive electrode separated by an ion exchange membrane. The battery uses electrodes that do not take part in the reactions but merely serve as substrates for the reactions. There is therefore no loss of performance, as in most rechargeable batteries, from repeated cycling causing electrode material deterioration.

In order to perform power system studies, there is a great need for properly validated models to correctly evaluate the amount and dynamic response of the storage [13]. The battery under test is located in the experimental facility of the Risø Campus of the Technical University of Denmark. The main aim of the tests is to provide an electrochemical characterization of the parameters in order to build a Thevenin equivalent [14,15].

The paper is developed as follows: Section 2 provides a description of the main aspects of the VRB technologies and analyzes the main electrochemical dynamics; Section 3 reports the experimental activity that is performed and the procedures adopted to evaluate the main characteristic parameters; Section 4 describes the comparison performed between the simulated model and the experimental tests; and Section 5 reports the conclusions and the further developments that are needed.

2. VRB dynamic model

The storage model presented and developed is suitable for electrical studies and has a general validity. The modeled dynamics consider the state of charge (SOC) behavior and electrochemical conversion. The main state variables are the state of charge, current, and voltage. All the characteristic elements of the storage system (open circuit voltage, internal resistances, limitations, and protections thresholds) present some kind of dependence on these state variables. Therefore, the relationships among them are investigated.

During operation, the two electrolytes flow from separate storage tanks to the cell stack where the reaction occurs. Ions transfer between the two electrolytes across the ion exchange membrane. After the reaction, the spent electrolytes flow back to the storage tanks.

The total power available is related to the electrode area within the cell stacks, while the total storable energy is a function of the tank volumes and the electrolyte concentrations [11–14]. The cells can have a current density of approximately 0.1 A cm^{-2}. Separate reactions occur in each half-cell: during discharge, electrons are produced in a negative half-cell reaction and are consumed in the positive half-cell reaction, forming the basis for an electrical current [16,17]. During discharge, in the negative half-cell, vanadium (II) ions in solution are converted to vanadium (III) ions, with the loss of an electron, which is available for conduction:

$$\overset{\text{CHARGED}}{V^{2+}} \underset{\text{CHARGE}}{\overset{\text{DISCHARGE}}{\longleftrightarrow}} \overset{\text{DISCHARGED}}{V^{3+}} + e^{-};\ E_0 = -0.255\ \text{V} \tag{1}$$

During discharge, in the positive half-cell, vanadium (V) ions are converted to vanadium (IV) ions, gaining an electron in the process:

$$\overset{\text{CHARGED}}{VO_2^+} + e^- + 2H^+ \underset{\text{CHARGE}}{\overset{\text{DISCHARGE}}{\longleftrightarrow}} \overset{\text{DISCHARGED}}{VO^{2+}} + H_2O;\ \ E_0 = 1.000\ \text{V} \tag{2}$$

The overall equation is as follows:

$$\overset{\text{CHARGED}}{VO_2^+} + 2H^+ + V^{2+} \underset{\text{CHARGE}}{\overset{\text{DISCHARGE}}{\longleftrightarrow}} \overset{\text{DISCHARGED}}{VO^{2+}} + H_2O + V^{3+},\ \ E_0 = 1.255 \tag{3}$$

Hydrogen cations are consumed in the process, which means that the pH of the positive electrolyte changes over time. To maintain the charge balance within the half-cells, there must be a mechanism for the transit of hydrogen ions from the negative half-cell to the positive half-cell, which is generally accomplished by placing an ion-conducting membrane between the two. The cell potential can be defined by the Nernst law:

$$V_{oc} = E_0 + \frac{R\cdot T}{n\cdot F}\ln\left[\frac{c_{V^{5+}}}{c_{V^{4+}}}\cdot c_{H^+}^2\cdot\frac{c_{V^{2+}}}{c_{V^{3+}}}\right] \tag{4}$$

where R is the ideal gas constant (equal to 8.314 J mol^{-1} K), F is the Faraday constant (equal to 95,484.56 C mol^{-1}), n is the number of moles of electrons transferred in the balance equation, and T is the absolute temperature (typically 298 K).

If it is assumed that the product/ratio of the activity coefficients is equal to 1, the potential E_0 can be assumed to be equal to 1.255 V, which is the sum of the negative and positive half-cell potentials during discharge. By defining the SOC as the measure of the level of energy stored, which is equal to 1 when the battery is fully charged and 0 when empty, the overall potential depends on the concentration ratios, c_v, of the electrolytes in the two tanks and, because of the linear dependence between these concentrations and SOC, the previous equation can be reformulated as described in Ref. [18]:

$$V_{oc} = E_0 + \frac{R\cdot T}{n\cdot F}\ln\left[\frac{SOC}{1-SOC}\cdot(SOC+6)^2\cdot\frac{SOC}{1-SOC}\right] \tag{5}$$

The battery's conceptual representation is based on the Thevenin equivalent model: a voltage source with a series resistance and RC chain. The voltage source and all the parameters are SOC and temperature dependant. The relationship will be determined by the experimental tests proposed further on.

One advantage of dealing with flow-based storage is the availability of the Open Circuit Voltage (OCV) measure at any time, which is provided by a dedicated measurement cell. The internal shunt losses, which are modeled by controlled current sources in parallel with the controlled voltage source that models the OCV, are typically about 3% of the battery's DC current [19–21].

The DC circuit is closed by a controlled voltage source that models the DC/DC chopper included in the DC/AC conversion system. This source sets the amplitude of the DC clamp voltage in order to achieve the desired AC power flow. The voltage set cannot exceed the lower and upper bounds to avoid cell damage. Inside the DC circuit, the Battery Management System (BMS) power consumption is also included. The Pulse Width Modulation (PWM) converter completes the conversion stage, and the power is thus available at the AC

connection point. The circulating pumps draw the required energy at this stage, upstream of the network interface [22].

It is assumed that all the cells that compose the battery are perfectly balanced, and thus the tasks requested of the storage system are equally divided among them. Under this assumption, all the dynamics are built into a single equivalent battery. The overall desired storage size is then obtained by multiplying/dividing the battery parameters by the number of series/parallel elements.

The block diagram presented in Fig. 1 can be read from the upper left to the lower right. The model input is the active power reference, PrefBattery (in pu or W), which is the power that the battery is asked to release or store. The output, PbatteryGrid, is the power effectively produced, including the power required by the auxiliary systems and the losses in the Power Conditioning System (PCS).

The power reference is passed through a first controller stage, which compares the request with the actual AC battery output, which means the power at the PCS connection, before the pump's withdrawal: the output is the dc reference current. This new reference is passed through a second control loop, called the Battery Current Controller, which sets the reference voltage that the DC side of the PCS has to set on the battery connection.

Inside this control loop, the extra signal, such as the max/min SOC level or max/min current, triggers the blocking of the storage. The applied voltage, subjected to a delay that models the PCS response time, is used in the Electrochemical Dynamic block to implement the storage dynamic model. A second-order model has been used with one time constant in the equivalent electrical circuit. Finally, the battery's DC output is evaluated, along with the internal shunt and Joule losses. With a knowledge of the converter efficiency curve and the auxiliary services consumption, it is possible to compute the storage power transit toward the grid.

3. Experimental procedures

3.1. Test setup

The analyzed VRB consists of a series of 3 stacks composed of 42 cells each, and it is equipped with two tanks containing 6500 L of vanadium solution each. Two circulating pumps move the liquid solutions along the pipes.

The system is interfaced to the local three-phase network through a bidirectional four quadrant 19-kVA PWM converter. The control and acquisition systems are based on an industrial PC running the linux OS, which collects all the measurements from the field. The electrical measurements are based on standard meters connected to the SCADA with a serial MODBUS protocol. The system polls all the meters every second, synchronizes the values, and stores the data in a real-time database.

Several tests (charge and discharge cycles) are performed. First, a complete discharge/charge cycle at nominal power (±15 kW AC) is carried out. The cycles are divided into 2-h steps, and after each step the storage power set-point is set to zero for 10 min in order to evaluate the internal dynamic resistance. The methodology and the results derived from these experiments are described in Sections 3.2, 3.3, and 3.4. For these charge/discharge paths, the efficiencies at the different energy conversion stages of the battery system are calculated and reported in Section 3.5.

Subsequently, a different approach is used to derive the dependence of the internal resistance, not only on the SOC, but also on the current intensity and sign. To do so, the battery is taken to different measured SOC levels (10%, 30%, 50%, 70%, and 90%), and at each point, a predefined DC reference current pattern is applied. The methodology and the results related to these activities are reported in Sections 3.6 and 3.7, respectively.

3.2. Discharge and charge at nominal power methodology measurements

Two tests are performed (one discharge and one charge) at 15 kW AC. The cycles are programmed so that the battery power output remains constant for 2 h, then is set to zero for 10 min and so on until the charge/discharge is complete:

- Discharge @ nominal power (15 kW AC → 16.2 kW DC) from 0% to 100% SOC level in 2-h steps. Time elapsed: 10 h and 25 min.
- Charge @ nominal power (−15 kW AC → −13.6 kW DC) from 0% to 100% SOC level in 2-h steps. Time elapsed: 18 h and 40 min.

The measured variables are the Battery Voltage, Reference Cell Voltage, Battery Current, and measured SOC. It has to be noted that the VRB, in contrast to other storage technologies, can provide an open circuit voltage using a reference cell. The estimation of the SOC value is thus performed in a very affordable and reliable way. The evaluated parameters are R_{static}, $R_{dynamic}$, $C_{dynamic}$, Max/Min Voltage thresholds, and the theoretical SOC. Fig. 2 reports the methodology adopted in order to evaluate the best time to measure the current and voltage.

The meaning of each measurement is reported here:

- V_{0-}: voltage @ t_{0-} (t_0 is the time when the voltage step occurs),
- V_{0+}: voltage @ t_{0+} (in reality it requires 2 s, one due to the inverter time constant and one due to the measurement delay),

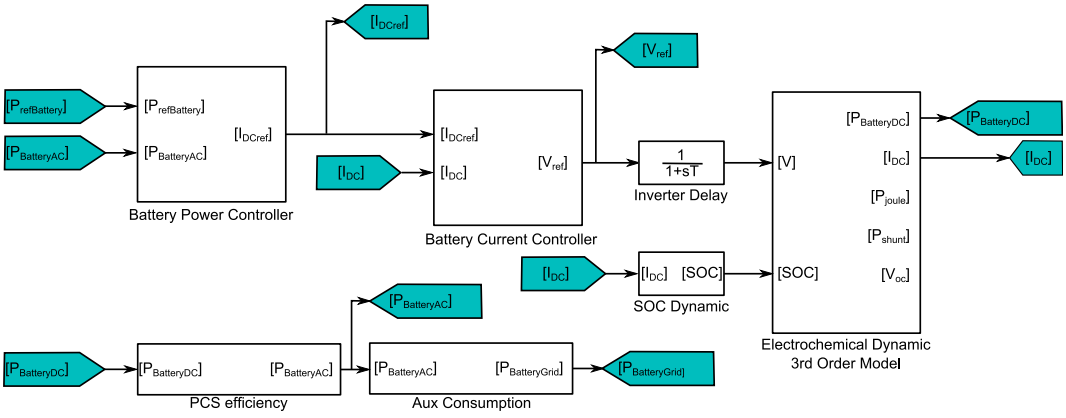

Fig. 1. VRB model block diagram.

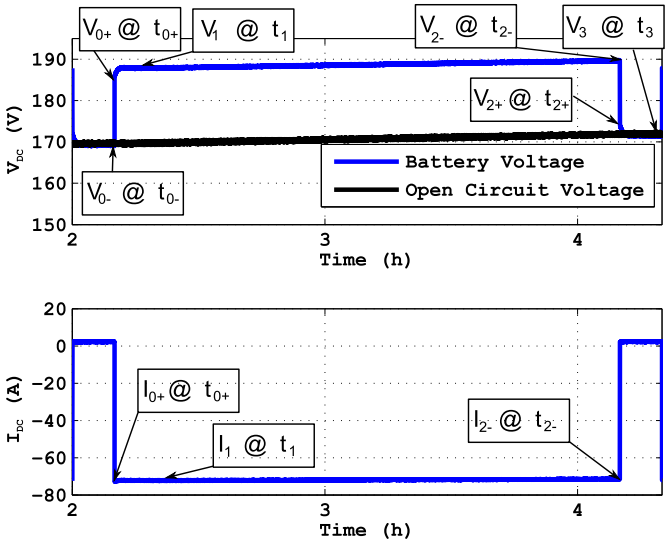

Fig. 2. Battery step response measurement procedures.

- V_1: voltage @ t_1 (t_1 is the time when the voltage reaches a steady state value),
- V_{2-}: voltage @ t_{2-} (t_2 is the time when the voltage step occurs),
- V_{2+}: voltage @ t_{2+} (in reality it requires 2 s, one due to the inverter time constant and one due to the measurement delay),
- V_3: voltage @ t_{inf} (in reality this is the voltage before the beginning of the next voltage step, it is equal to the V_{0-} of the following step),
- I_{0+}: current @ t_{0+},
- I_1: current @ t_1,
- I_{2-}: current @ t_{2-}.

With these measurements, the parameters are determined as follows (see Fig. 3):

- R_{static_begin}: $|(V_0 - V_{0+})/I_{0+}|$,
- R_{static_end}: $|(V_2 - V_{2-})/I_{2-}|$,
- 3τ: the time required for the voltage to get inside the band $(V_3 \pm 0.05 \cdot |V_3 - V_{2-}|)$,
- V_1: the value the voltage reaches after $t_{0+} + 3\tau$,
- $R_{dynamic}$: $|(V_1 - V_{0+})/I_1|$,
- $C_{dynamic}$: $\tau/R_{dynamic}$

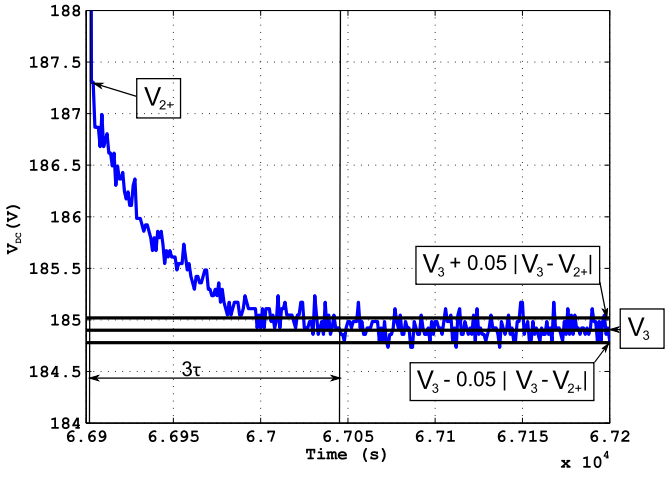

Fig. 3. 3τ evaluation.

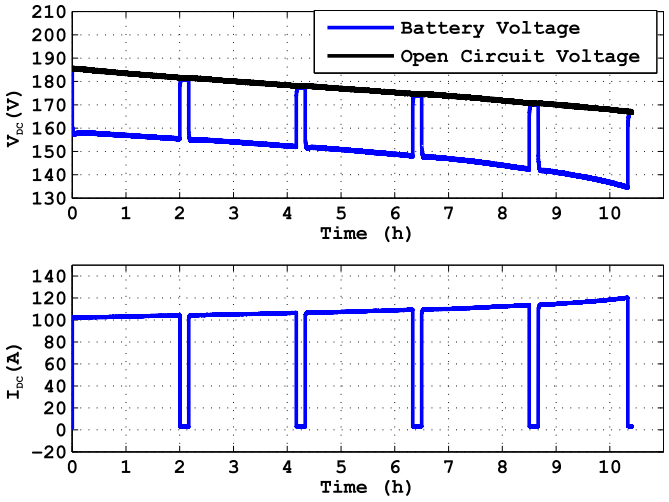

Fig. 4. OCV and battery voltages and currents.

Once all the parameters are evaluated, the electric circuit can be fully characterized.

It is worth noting that, in the battery under study, the pumps' consumption is about 1500 W when the battery is running at full power and 1400 W when the power is reduced (1/3 of the nominal). If the battery is in stand-by, but ready to enter into service, the consumption still remains high (about 1150 W). Moreover, the Battery Management System (BMS) is always on and constantly requires about 400 W.

3.3. Discharge at nominal power results

The first test performed is the discharge at nominal power (15 kW AC side → 16.2 kW DC side). Every 2 h, discharging is stopped for 10 min in order to evaluate the dynamic parameters (internal RC chain). This test lasts 10 h and 25 min, and supplies 156.22 kWh (DC side) and 145 kWh (AC side).

Figs. 4 and 5 report the measured voltages, current, powers, and SOC during the discharge. If the OCV values given by the reference cell are plotted as a function of the measured SOC, it can be noted that the internal BMS gives information about an SOC that does not correspond to the theoretical OCV–SOC relationship described by the Nernst law, here reported in Fig. 6.

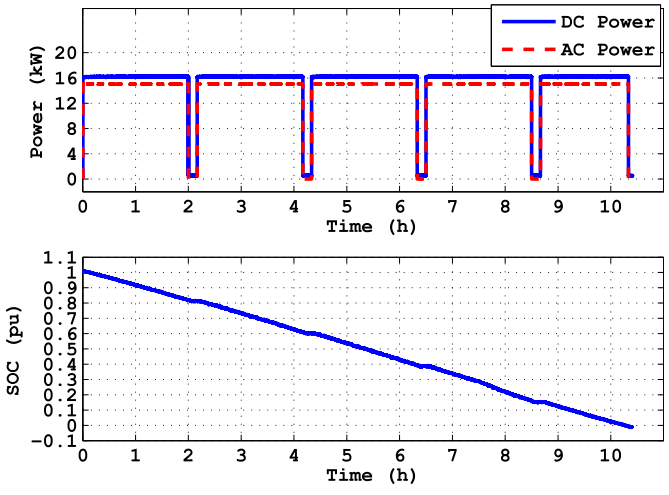

Fig. 5. DC and AC powers and SOC.

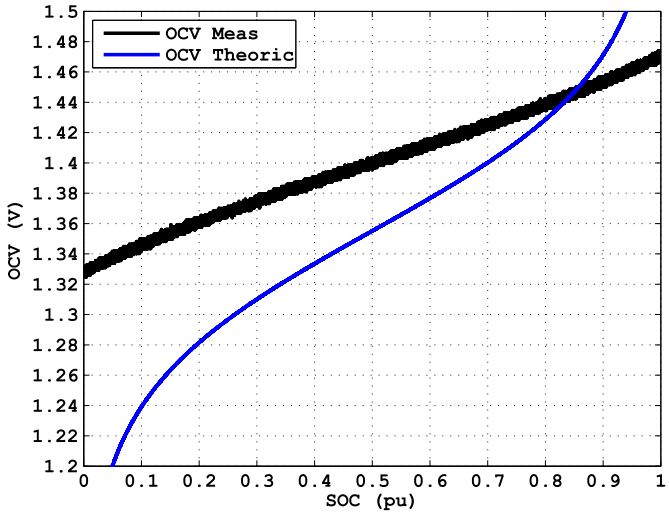

Fig. 6. OCV measured by reference cell and OCV calculated by Nernst law.

It is thus deduced that the SOC values that the BMS reports differ from the real SOC value. The battery operates in a range that is considerably smaller than its maximum potential, well inside the linear segment of the characteristic. In order to evaluate the real SOC values that the storage reaches, and thus estimate its real energy capacity, it has been built with an OCV–SOC characteristic that fits the theoretical one described by the Nernst law.

The energy stored in the battery is calculated as follows:

$$E_{SOC} = E_{DC} - E_{BMS} - E_{Joule} - E_{Shunt} \quad (6)$$

where E_{DC} is the energy measured on the DC side, known as the integral of the DC power; E_{BMS} is the energy need of the BMS, known as the integral of the assumed constant 400-W consumption; E_{Joule} is the energy lost as a result of the Joule effect on the internal resistances (both static and dynamic); and E_{Shunt} is the energy lost as a result of the shunt currents, estimated as the integral of a percentage (3%) of the DC power.

The "true" SOC step is calculated as E_{SOC}/E_{nom}, where E_{nom} is an estimation of the battery capacity based on the size of the tanks and the technology energy density (around 25 Wh l^{-1}).

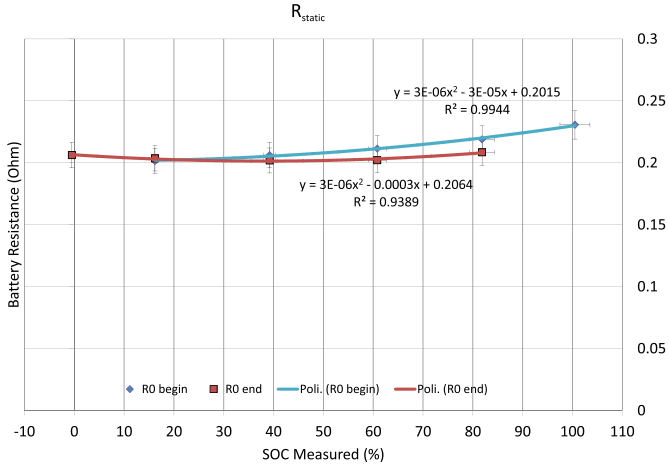

Fig. 7. R_{static}, $C_{dynamic}$, and $R_{dynamic}$ as functions of measured SOC.

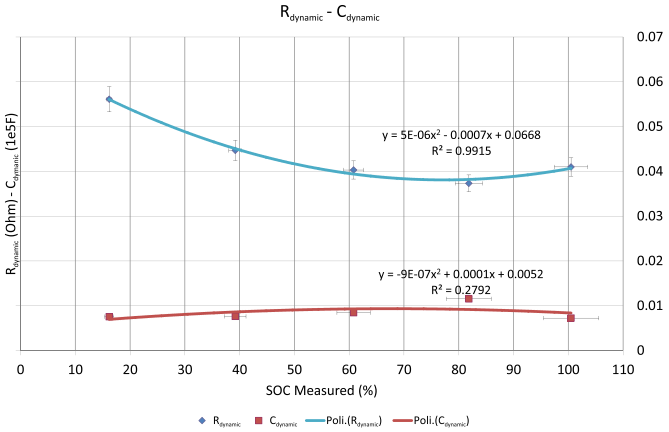

Fig. 8. $C_{dynamic}$ and $R_{dynamic}$ as functions of measured SOC (R in Ohm, C in 1e5 F).

The OCV is then calculated using the Nernst law based on the "true" SOC value. The objective is to overlap the curve with the measured OCV by modifying the initial SOC and battery capacity.

At the end of the process, the estimated values are as follows:

- $E_{nom} = 320$ kWh
- $E_{SOC} = 193$ kWh

The energy stored in the battery is equal to around 193 kWh, thus corresponding to 60% (from 18% to 78%) of the estimated battery capacity (i.e., 320 kWh). The internal BMS significantly reduces the possible working range.

The evaluated parameters, R_{static}, $R_{dynamic}$, and the time constant (and thus $C_{dynamic}$) are reported as functions of the measured SOC in Figs. 7 and 8. The internal static resistance shows a slight dependence on the SOC (±15% around the average value) and is higher at low and high SOC levels. The dynamic resistance is almost constant at time constant values of around 40 s.

The temperatures are also measured (see Fig. 9). In this case, five sensors are applied to the stack, measuring the inlet liquid pipe for the cell, the outlet liquid pipe for the cell, the stack top temperature, and the room temperature at two different positions.

All the temperatures remain sufficiently constant (see Fig. 9). Moreover, the difference between the inlet and outlet temperatures is very low. Therefore, we infer that there is no need to correlate the storage system parameters with temperature, at least under the operation conditions allowed by the BMS. The temperature profiles also indicate that the output power of the inverter is well below the actual power capability of the battery cell stacks.

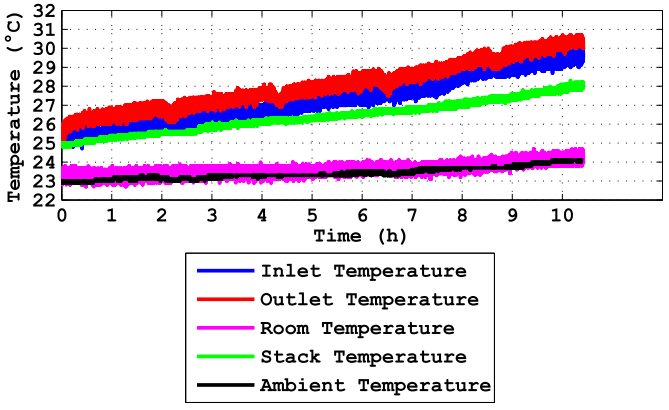

Fig. 9. Temperatures during discharge at nominal power (15 kW AC).

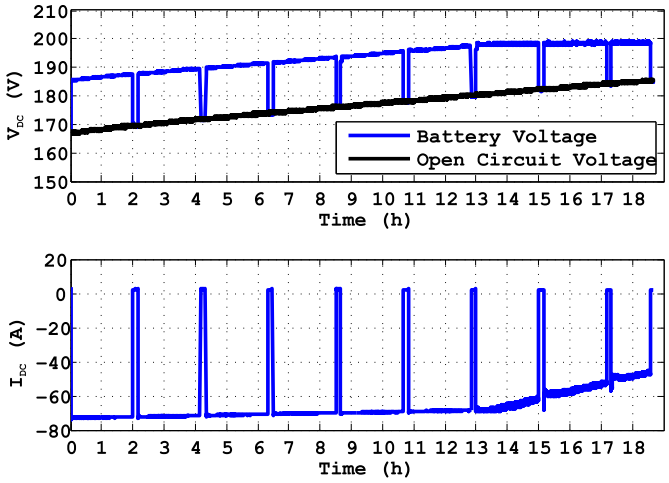

Fig. 10. OCV and battery voltages and currents.

3.4. Charge at nominal power results

The second test performed is charging at nominal power (−15 kW AC side → −13.6 kW DC side). Every 2 h, the charging is stopped for 10 min in order to evaluate the dynamic parameters (internal RC chain). This test lasts 18 h and 40 min, and leads to stored energy equal to 246.1 kWh (AC side) and 222.6 kWh (DC side).

Figs. 10 and 11 present the measured voltages, currents, powers, and SOC during the charge.

It can be noted that once the SOC reaches high levels, the voltage required to push energy inside the battery would be too high, damaging the cells. The BMS sets a maximum voltage threshold of 199 V (this represents 1.58 V per cell), leading to a reduction in the recharging current and power.

The same procedures described for the discharge are applied for the charge. At the end of the process, the estimated values are as follows:

- $E_{nom} = 320$ kWh
- $E_{SOC} = 189$ kWh

In this case, the energy stored in the battery is equal to around 189 kWh, which is very similar to the value obtained in the discharge case. Thus, the usable energy from BMS is shown to be about 190 kWh.

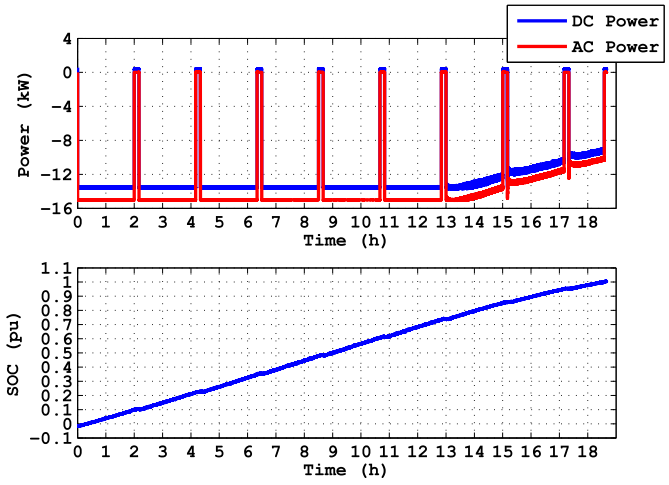

Fig. 11. DC and AC powers and SOC.

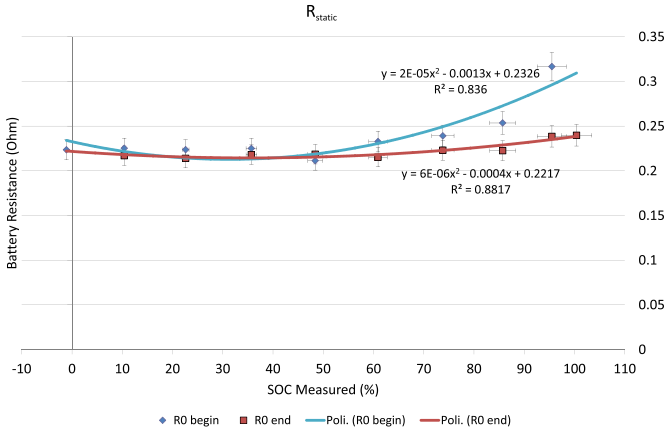

Fig. 12. R_{static} as function of measured SOC.

The evaluated parameters R_{static}, $R_{dynamic}$, and the Time constant (and thus $C_{dynamic}$) are hereafter reported in Fig. 12 and in Fig. 13 as functions of the measured SOC.

During the charge, the parameters show a slight dependence on the SOC. Moreover, the values are higher than those obtained during the discharge. Because of this, further tests aimed at a better characterization of the dependence on the intensity and the sign of the current are performed.

From the thermal perspective, the charge is less demanding than the discharge; because of the minor current level on the DC side, the temperatures do not even increase (Fig. 14).

3.5. System efficiencies

There are different efficiencies for different parts of the storage system. Fig. 15 helps to clarify these efficiency stages. η_{DC} is useful for analyzing the electrochemical performances of the storage because it includes the Joule and shunt losses. The Joule losses account for the losses on the internal series resistance, whereas the shunt losses take into consideration the solution leakage across the cells.

η_{AC} measures the PCS efficiency, while η_{pumps} gives an indication of the consumption of the main auxiliary system (i.e., the circulating pumps) compared to the power transit inside and outside of the storage. η_{system} is the global product of the efficiencies just described.

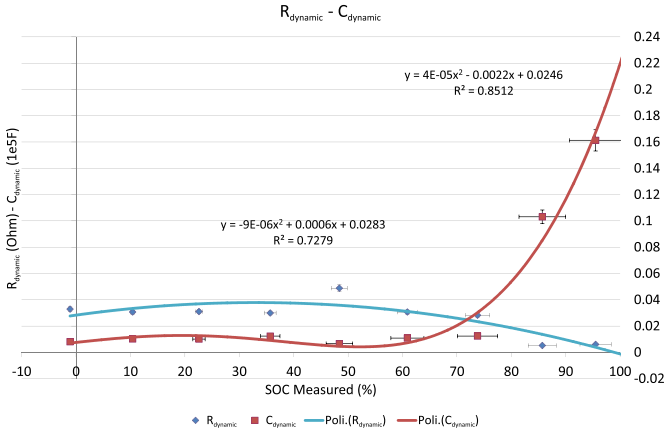

Fig. 13. $C_{dynamic}$ and $R_{dynamic}$ as functions of measured SOC (R in Ohm, C in 1e5 F).

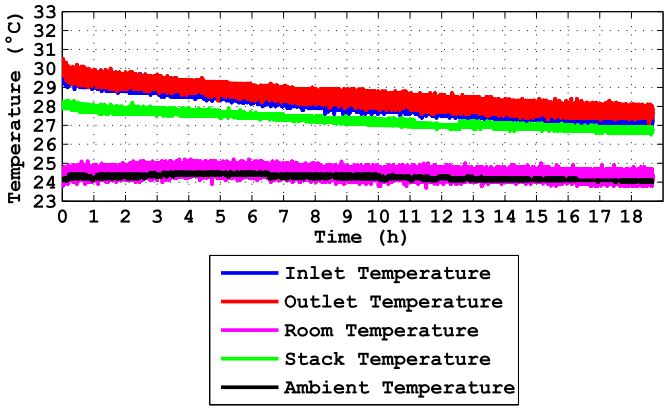

Fig. 14. Temperatures during charge at nominal power (−15 kW AC).

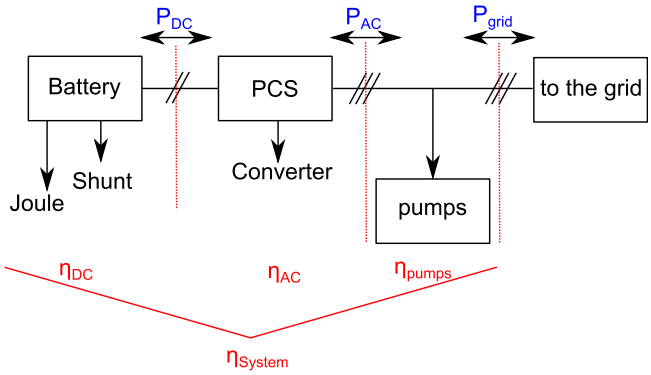

Fig. 15. System efficiencies.

Particular attention must be given to the definitions of the efficiencies. Generally, the system efficiency is the ratio between the output energy and the input energy. However, because of the reversibility of the storage, the method used to compute the efficiencies changes accordingly. Different formulas are thus defined for the discharge (i.e., positive power) and charge (i.e., negative power):

$$\begin{cases} P_{DC} \geq 0 \rightarrow \eta_{DC} = P_{DC} / \left(P_{DC} + P_{Joule} + P_{Shunt} \right) \\ P_{DC} < 0 \rightarrow \eta_{DC} = \left(P_{DC} - P_{Joule} - P_{Shunt} \right) / P_{DC} \end{cases} \quad (7)$$

$$\begin{cases} P_{AC} \geq 0 \rightarrow \eta_{AC} = P_{AC} / P_{DC} \\ P_{AC} < 0 \rightarrow \eta_{AC} = P_{DC} / P_{AC} \end{cases} \quad (8)$$

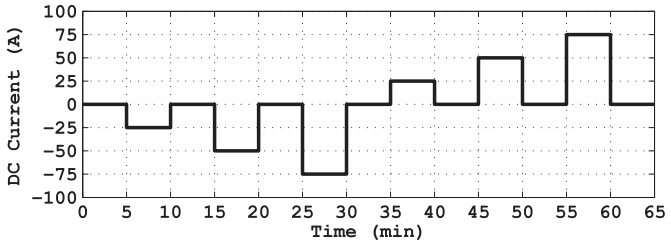

Fig. 16. Battery current steps.

$$\begin{cases} P_{Pumps} \geq 0 \rightarrow \eta_{Pumps} = P_{Grid} / P_{AC} \\ P_{Pumps} < 0 \rightarrow \eta_{Pumps} = P_{AC} / P_{Grid} \end{cases} \quad (9)$$

$$\eta_{System} = \eta_{DC} \eta_{AC} \eta_{Pumps} \quad (10)$$

Table 1 summarizes the obtained results regarding the achieved energy values and related stage efficiencies.

It is thus possible to make a rough evaluation of the roundtrip efficiencies:

- **DC roundtrip**: 156.2 kWh discharged vs. 222.6 kWh charged → DC_eff = 70.2%,
- **AC&DC roundtrip**: 145.0 kWh discharged vs. 246.1 kWh charged → AC_eff = 58.9% (because of DC_eff, the inverter efficiency, and the BMS losses),
- **Full roundtrip**: 129.7 kWh discharge vs. 273.5 kWh charged → Full_eff = 47.4% (because of the previous efficiencies and the consumption of the pumps).

It has to be noted that these efficiencies do not take into account the fact that the BMS and pumps also run when the battery is in stand-by, ready to work.

It can be noted that, regarding the DC efficiency, the VRB studied benefits from the fact that the inverter (and thus the maximum power transit) is downsized compared to the cell capability, which leads to a relatively high value. However, if the maximum current could be applied, the efficiency value obtained would not be very high compared to other storage technologies (i.e., lithium-ion). The AC efficiency might be increased by using a newer PWM inverter: 96% efficiency is easily achievable today for a small-size transformer-less inverter.

Concerning the pumps, they are a constant-power type, which require almost the same power despite the battery production. They could benefit from inverter-driven modulation because the amount of liquid required in the reaction is proportional to the amount of power transit requested. This means that during a light power condition, it is useless to have the pumps running at maximum power.

3.6. Current step methodology measurements

Because it has been noted that the internal resistance is a function of the SOC and the sign of the current, the dependence on

Table 1
Energy and efficiency assessment.

	Σ E_{SOC} [kWh]	Σ E_{Shunt} [kWh]	Σ E_{Joule} [kWh]	Σ E_{BMS} [kWh]	Σ E_{DC} [kWh]	Σ E_{AC} [kWh]	Σ E_{pumps} [kWh]	Σ E_{grid} [kWh]
Discharge	193.4	4.7	28.6	3.9	156.2	145.0	15.2	129.7
Charge	188.5	6.7	20.5	6.9	222.6	246.1	27.4	273.5
	η_{DC}	η_{AC}	η_{pump}	η_{sys}			Time elapsed	
Discharge	80.8%	92.8%	89.5%	67.1%			10:25 h	
Charge	84.7%	90.5%	90.0%	68.9%			18:40 h	

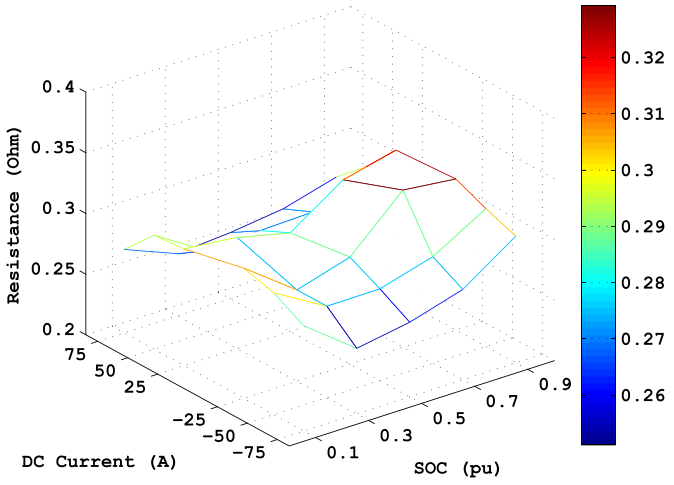

Fig. 17. R_{static} functions of SOC and DC current.

the current intensity is also investigated. To do this, a measurement campaign is performed according to the following procedures: the battery is taken to different measured SOC levels (10%, 30%, 50%, 70%, and 90%), and at each point, the DC reference current pattern, shown in Fig. 16, is set into the BMS.

The shortness of the charge/discharge cycles and the oversizing of the cell stack (compared to the inverter size) do allow the temperature variation to be within a few degrees. Thus, the measurements hereafter reported are for a constant temperature. For each current step, the internal resistance is evaluated as the ratio of the DC voltage drop (the battery voltage is measured while the OCV is available from the reference cell) and the DC current (calculated as the ratio of DC power and battery voltage). It has to be noted that the electrochemical delay (the one modeled as the RC chain) cannot be avoided. Thus, the steps are 5 min long in order to be able to reach a steady state.

3.7. Current step results

In Figs. 17 and 18, the static resistance and dynamic resistance values as functions of both the SOC and DC current are depicted. In order to better show the dependences, two different views are proposed.

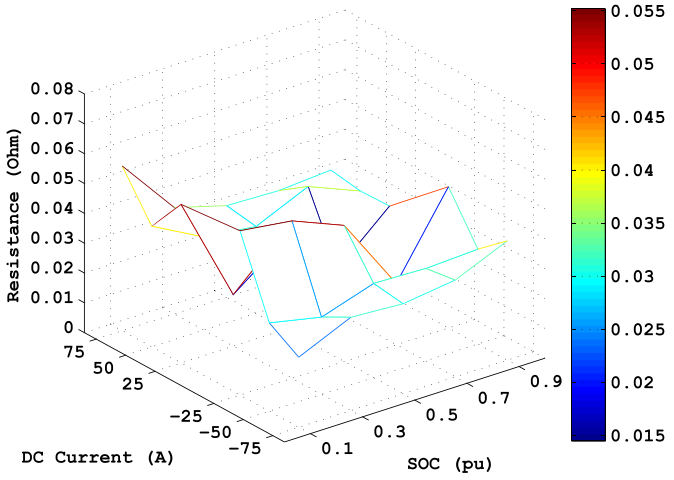

Fig. 18. $R_{dynamic}$ as function of SOC and DC current.

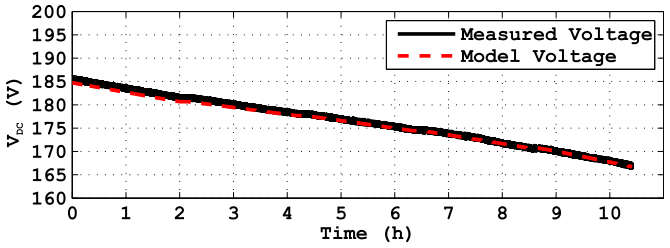

Fig. 19. Measured and model open circuit voltages.

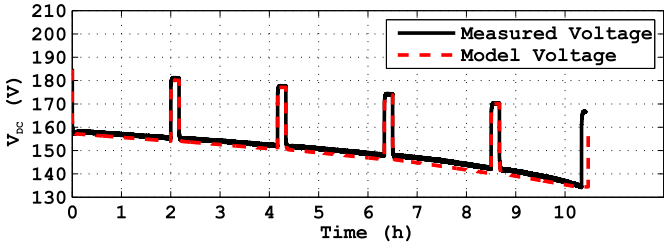

Fig. 20. Measured and model battery voltages.

It is worth noting that the global and static resistance functions have a saddle-like shape, which indicates higher resistance values at low and high SOC levels, with small intensity currents. On the other hand, the dynamic internal resistance does not seem to have any remarkable correlation with the current intensity. In addition, because it is ten times smaller than the static component, measurement errors may affect the calculations.

4. Model validation

4.1. Discharge paths

This section shows how the previously described charge and discharge tests were repeated using the Simulink model

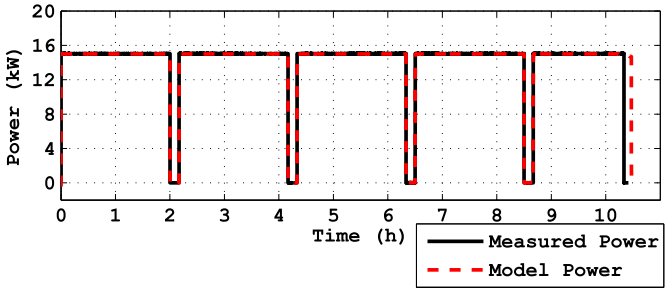

Fig. 21. Measured and model AC powers.

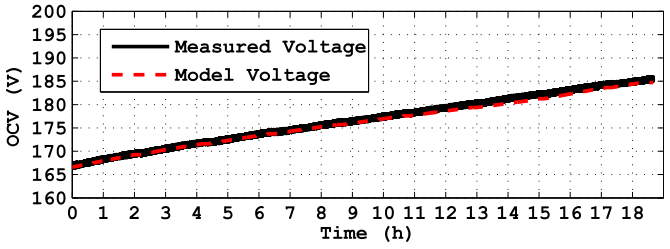

Fig. 22. Measured and model open circuit voltages.

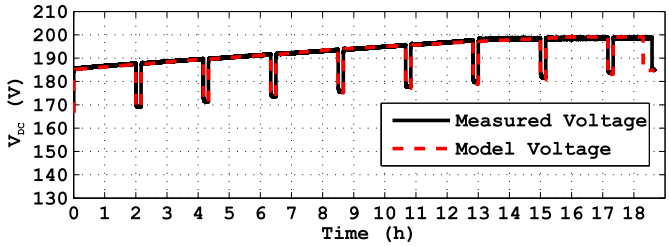

Fig. 23. Measured and model battery voltages.

characterized by the obtained parameter data. The results are compared with the results collected during the testing campaign. Fig. 19 reports the open circuit voltage obtained during the test and that of the model. The relative error is lower than or equal to 1%.

Fig. 20 shows the battery voltage. Moreover, in this case, the matching is very good, and the errors are within ±2%. Finally, the AC profile is reported in Fig. 21.

4.2. Charge paths

The same comparison is also performed for the charge test. The results for the voltages are reported in Figs. 22 and 23. A good match can again be found.

Some differences can be found in the AC profile (Fig. 24), especially when the battery hits the maximum voltage threshold. Nevertheless, the differences are in the range of ±10%. The reason for this can probably be found in the battery system internal controller, which is modeled with a proportional integral controller and presents some features that would require further analysis to be properly modeled.

5. Conclusions

The present work focused on the development of a model of a VRB storage system suitable for electrical studies, using the Matlab-Simulink environment. The model validation was performed with a real device installed in the SYSLAB test facility of DTU Risø Campus.

The electrochemical dynamic model of a Vanadium Redox Flow was proposed and analyzed from the electrochemical perspective, including all the limitations and the protection systems. All the dynamics were built into the equivalent cell, and the desired size of the storage system could be obtained by multiplying the cell parameters by the number of series/parallel elements. The storage model was realized and described in order to provide general validity, even though, in the present study, it was tailored for specific chemistries.

The usable energy was around 190 kWh compared to a theoretical energy of 320 kWh. The internal resistances had a dependence on SOC and the sign and intensity of the current. Higher values were achieved during a charge at low intensity, while lower ones were found during the full power discharge. Moreover, there was a slight reduction whenever the measured SOC was within the central area. A thermal measurement campaign made it possible to determine that the cell stack was oversized compared to the inverter. Thus, the VRB thermal overload capability could not be properly assessed. An evaluation of the storage efficiencies was also performed. Several efficiencies were defined depending on the subsystem considered. The analyzed model was compared with the same charge/discharge paths adopted during the experimental test. A good matching of the main variables was obtained, even though some mismatches arose. Further model improvements will aim at better characterizing the response during the charge limitations periods.

The tests were useful to determine the internal parameters and system efficiencies. They also provided indications about which conversion stage aspects the manufacturer should focus on in order to improve the overall efficiency. The testing procedures presented are going to be replicated in the lithium ion storage installed in the electric cars present in the test facility in order to validate proper dynamic models for this technology as well.

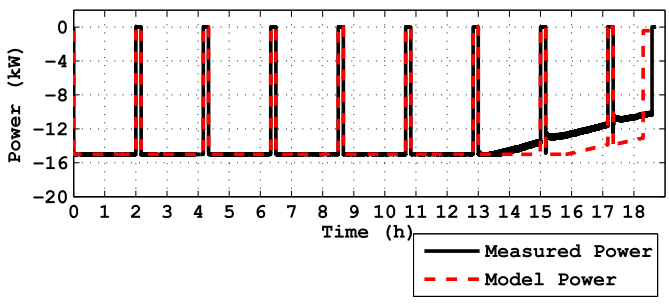

Fig. 24. Measured and model AC powers.

Acknowledgments

This work was supported in part by EU Funding through the DERRI Project under grants ID 20110531-02 (Wind Power and Storage Modeling and Integrated Control in Electric Distribution systems) and ID 20110531-04 (Renewable Energy Sources and Storage for Integrated Control in Electric Distribution Systems), coordinated by Dr. F. Silvestro (University of Genova).

References

[1] C.A. Hill, M.C. Such, C. Dongmei, J. Gonzalez, W.M. Grady, IEEE Trans. Smart Grid 3 (2012) 850–857.
[2] A. Oudalov, D. Chartouni, C. Ohler, G. Linhofer, in: Proc. Power Syst. Conf. Expo., 2006, pp. 2206–2211.
[3] D. Di Rosa, I. Fastelli, G. Gigliucci, S. Grillo, M. Marinelli, S. Massucco, F. Silvestro, in: Integration of Renewables into the Distribution Grid, CIRED Workshop, 2010, pp. 1–4.
[4] K.C. Divya, J. Østergaard, Electr. Power Syst. Res. 79 (2009) 511–520.
[5] Electric Energy Storage Technology Options: a White Paper on Applications, Costs and Benefits, EPRI Corp, Palo Alto, CA, Dec. 2010. Tech. Rep. 1020676.
[6] H. Ibrahim, A. Ilinca, J. Perron, Renew. Sustain. Energy Rev. 12 (2008) 1221–1250.
[7] S. Grillo, M. Marinelli, S. Massucco, F. Silvestro, IEEE Trans. Smart Grid 3 (2012) 950–958.
[8] Vanadium Redox Flow Batteries: an In-depth Analysis, EPRI Corp., Palo Alto, CA, 2007. Tech. Rep. 1014836.
[9] T. Shigematsu, T. Kumamoto, H. Deguchi, T. Hara, Proceedings of IEEE Power Engineering Society Transmission and Distribution Conference and Exhibition: Asia Pacific, 2002, pp. 1065–1070.
[10] M. Skyllas-Kazacos, C. Menictas, in: Telecommunications Energy Conference, INTELEC 97, 1997, pp. 463–471.
[11] B. Turker, S.A. Klein, E. Hammer, B. Lenz, L. Komsiyska, Energy Convers. Manage. 66 (2013) 26–32.
[12] F. Baccino, M. Marinelli, F. Silvestro, O. Camacho, F. Isleifsson, P. Nørgård, in: Integration of Renewables into the Distribution Grid, CIRED Workshop, 2012, pp. 1–4.
[13] A. Tang, S. Ting, J. Bao, M. Skyllas-Kazacos, J. Power Sources 203 (2012) 165–176.
[14] M. Chen, G.A. Rincón-Mora, IEEE Trans. Energy Convers. 21 (2006) 504–511.
[15] S. Grillo, M. Marinelli, F. Silvestro, Wind turbines integration with storage devices: modelling and control strategies, in: Ibrahim Al-Bahadly (Ed.), Wind Turbines, 2011.
[16] C. Ponce de León, A. Frías-Ferrer, J. González-García, D.A. Szánto, F.C. Walsh, J. Power Sources 160 (2006) 716–732.

[17] C. Menictas, M. Skyllas-Kazacos, J. Appl. Electrochem. 41 (2011) 1223–1232.
[18] C. Blanc, A. Rufer, in: Proceedings of IEEE International Conf. on Sustainable Energy Technologies, 2008, pp. 696–701.
[19] E. Micolano, M. Broglia, L. Mazzocchi, C. Bossi, GENDIS Tech. Rep. in Italian A5-053120, 2005, pp. 1–51.
[20] M. Marinelli, S. Massucco (supervisor), F. Silvestro (supervisor), Wind Turbine and Electrochemical Based Storage Modeling and Integrated Control Strategies to Improve Renewable Energy Integration in the Grid, Ph.D. thesis, University of Genova, 2011.
[21] J. Chahwan, C. Abbey, G. Joos, in: Proceedings of IEEE Canada Electrical Power Conference, 2007, pp. 387–392.
[22] F. Baccino, S. Grillo, M. Marinelli, S. Massucco, F. Silvestro, in: Proc. 2nd IEEE Power Engineering Society Conference and Exhibition on Innovative Smart Grid Tech., 2011, pp. 1–8.